

*Supporting Information for*

## **Deactivation mechanisms of Ni-based tar reforming catalysts as monitored by X-ray absorption spectroscopy<sup>#</sup>**

Matthew M. Yung<sup>a,\*</sup> and John N. Kuhn<sup>b,\*</sup>

<sup>a</sup> National Bioenergy Center, National Renewable Energy Laboratory, 1617 Cole Boulevard, Golden, Colorado 80401

<sup>b</sup> Department of Chemical & Biomedical Engineering, University of South Florida, 4202 East Fowler Avenue, ENB 118, Tampa, FL 33620

<sup>#</sup> **Invited manuscript honoring Gabor A. Somorjai 75<sup>th</sup> birthday**

\* To whom correspondence should be addressed. E-mail: [matthew\\_yung@nrel.gov](mailto:matthew_yung@nrel.gov) and [jnkuhn@usf.edu](mailto:jnkuhn@usf.edu)

### **Experimental Section**

#### *1. Catalyst Synthesis*

The catalyst support, AD90 (CoorsTek Ceramics), consisted of 90.3 wt%  $\alpha$ -Al<sub>2</sub>O<sub>3</sub> with a specified mixture of other oxides (including SiO<sub>2</sub>, MgO, CaO, BaO, Na<sub>2</sub>O, Fe<sub>2</sub>O<sub>3</sub>, K<sub>2</sub>O, and TiO<sub>2</sub>) making up the remaining portion. The AD90 support had a surface area of 0.75 m<sup>2</sup>/g with an average particle size of 140  $\mu$ m. Single-solution incipient wetness impregnation of nickel, magnesium, and potassium nitrate precursors was used to add 6.1 wt% Ni, 2.4 wt% Mg, and 3.9 wt% K to the support. Two impregnations were conducted with 2 hr calcinations at 650 °C in air following each impregnation. This procedure resulted in a catalyst, referred to as Catalyst 50, with a nominal calcined composition of 6.6%NiO/3.4%MgO/4.0%K<sub>2</sub>O/AD90.

## *2. Kinetic Experiments*

The raw syngas stream sent to the catalytic reactor was created via indirect steam gasification of biomass. A steam-to-biomass ratio of 1:1 (15 kg/h H<sub>2</sub>O, 15 kg/h white oak chips) was used to create the syngas, with an average composition shown in Table S1. The kinetic experiments were conducted in a 35.6 cm (14”) ID fluidized bed reactor loaded with 60 kg of catalyst. Tar content was determined using a molecular beam mass spectrometer (MBMS) for direct analysis of gases leaving the reactor. Following a dodecane scrubbing unit used to remove steam and condensable tars, light gases were analyzed using gas chromatography and nondispersive infrared spectroscopy.

The oxidized-form of the catalyst was activated through H<sub>2</sub> reduction to create a reduced-form catalyst before it was exposed to reaction gases to create a post-reaction sample. The post-reaction catalyst was then regenerated using steam and air. This process was repeated for ten reaction cycles, with catalyst samples collected at each stage in the process, as depicted in Scheme 1. Additional details about catalyst preparation, the reaction system, and reaction conditions have been previously reported <sup>1</sup>.

## *3. XAFS at Advanced Photon Source (Argonne National Laboratory)*

X-ray absorption fine structure (XAFS) spectroscopy was performed at DuPont-Northwestern-Dow (DND) Collaborative Access Team (CAT) beamline 5-BM-D (BM = bending magnet, <http://www.dnd.aps.anl.gov/>) at the Advanced Photon Source, Argonne National Laboratory.

During the run, the storage ring energy and circulating current were 7.0 GeV and 100.6 mA, respectively. X-rays were selected using a Si(111) monochromator. For acquisition of the XAFS data, catalyst powders (a mass  $\sim$  125 mg) were ground with a mortar and pestle and pressed onto 13 mm diameter pellets using a Carver press operated at 12,500 psi for 20 s. Pellet thicknesses were adjusted to obtain a linear absorption coefficient near 1. Spectra were collected in transmission mode at the Ni K absorption edge (8333 eV) under ambient conditions. Energies were scanned from 150 eV before to 30 eV before the edge in 10 eV steps (background region) and then to 975 eV (representing  $k = 16 \text{ \AA}^{-1}$ ) after the edge in 2 eV steps (pre-edge/edge region). The absorption was measured using ionization chambers before and after the sample. Following the second ionization chamber, a Ni foil and a third ionization chamber were positioned so this reference could be examined simultaneously. Multiple scans (typically 3 or 4 per sample) were taken to improve the signal-to-noise ratio. Merging of individual scans and data reduction were performed with the Athena software package <sup>2-3</sup>. The background region (-150 to -30 eV before the edge) was extrapolated and subtracted from the data. Edge energies were selected as energy yielding the maximum absorption derivative. Spectra were normalized with a polynomial spline operation by the absorption over the  $\Delta k$  range of 6 to 15  $\text{\AA}^{-1}$ . Finally, the spectra were Fourier transformed with a Hanning window from  $k$ -space into  $R$ -space over the  $\Delta k$  range of 3 to 12  $\text{\AA}^{-1}$ .

### **Quantitative analyses of EXAFS results**

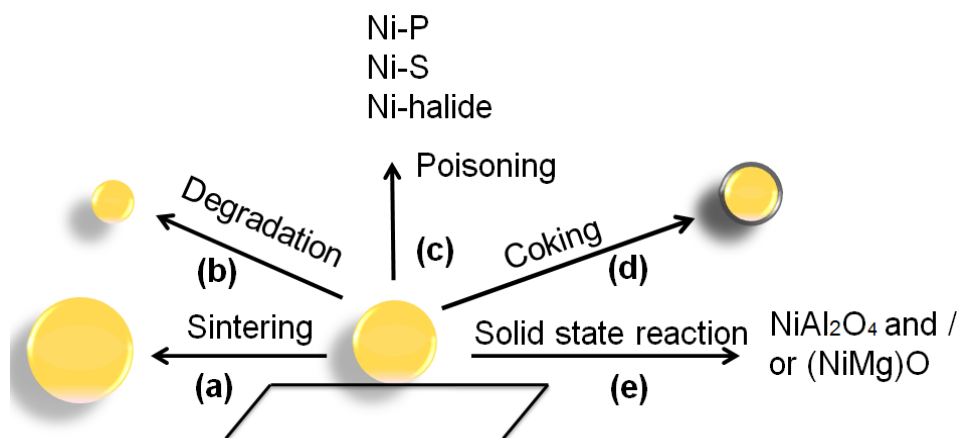
The three qualitative models developed in the previous section will now be quantitatively developed and assessed. The fittings were mathematically implemented using Artemis and its underlying codes <sup>2,4</sup>, which were used to calculate theoretical backscattering phases, amplitudes,

and phase corrections. The data range in k-space was  $\Delta k$  of 3 to 12  $\text{\AA}^{-1}$  for the Fourier Transform in R-space. Fittings were performed in R-space over  $\Delta R$  of 1 to 3.5  $\text{\AA}$  (for 14 independent points) using k-weights of 1, 2, and 3. The Ni-Ni path was used for phase corrections. Coordination numbers (CN), interatomic distances between an absorber and backscatter pair (R), mean-square displacements in the distribution of interatomic distances ( $\sigma^2$ ), amplitude reduction factors ( $\sigma_o^2$ ), and inner potential corrections ( $\Delta E_o$ ) were the parameters determined from modeling the EXAFS data.

Analysis of the Ni foil (FCC metal;  $CN_{Ni-Ni} = 12$ ) led to a  $R_{Ni-Ni}$  of 2.48  $\text{\AA}$  and a R-factor of 1.7% with the other parameters as follows:  $\sigma^2 = 0.0072 \text{ \AA}^2$ ,  $\sigma_o^2 = 0.81 \text{ \AA}^2$ , and  $\Delta E_o = -8.65 \text{ eV}$ . Analysis of the NiS ( $CN_{Ni-S} = CN_{Ni-Ni} = 5$ ) led to a  $R_{Ni-S}$  of 2.28  $\text{\AA}$  ( $\sigma^2 = 0.0065 \text{ \AA}^2$ ,  $\sigma_o^2 = 1.58 \text{ \AA}^2$ , and  $\Delta E_o = 0.077 \text{ eV}$ ) and  $R_{Ni-Ni}$  of 2.54  $\text{\AA}$  ( $\sigma^2 = 0.0070 \text{ \AA}^2$ ,  $\sigma_o^2 = 0.84 \text{ \AA}^2$ , and  $\Delta E_o = 1.16 \text{ eV}$ ) with a R-factor of 1.3%. Assessment of a Ni-O phase was evaluated by shell adding a Ni-O shell with a Ni-Ni shell. Due to the many possible oxide phases with Ni-Al-Mg present, there was no attempt to capture the exact phase since the interatomic distances of Ni-O in various phases are similar (e.g., NiO<sup>6-9</sup>, (Ni,Mg)O<sup>6</sup>, NiAl<sub>2</sub>O<sub>4</sub><sup>7,10</sup> and (Ni,Mg)Al<sub>2</sub>O<sub>4</sub> all have a similar Ni-O spacing) and the number of independent points limited the number of shells to be simultaneously evaluated to the point that meaningful results could not be obtained. Coordination numbers were determined by approximating the amplitude reduction factor of the catalyst samples to those obtained by the reference materials. Only fits with reasonable values for  $\Delta E_o$  (less than  $\sim|10 \text{ eV}$ ) and  $\sigma^2$  (less than  $\sim 0.02 \text{ \AA}^2$ ) were considered. Coordination numbers were optimized to obtain an amplitude reduction factor ( $\sigma_o^2$ ) similar as to the values obtained above for the specific absorber-backscatter pairs in reference materials. Uncertainty in coordination numbers were 0.25 for Ni-

Ni spacings and 0.05 for all other absorber-backscatter pairs. R-factors less than ~2%, as obtained for the reference materials, were generally used to signify a good fit.

## Supporting Data



**Scheme S1: Potential deactivation mechanisms for catalyst system under investigation.**

**Table S1: Average inlet composition of biomass-derived syngas sent to the catalytic reactor.**

Average Inlet Composition	
vol% (H <sub>2</sub> O-, N <sub>2</sub> -free basis)	
H <sub>2</sub>	33
CO	24
CO <sub>2</sub>	22
CH <sub>4</sub>	13
C <sub>2</sub> H <sub>4</sub>	3
C <sub>2</sub> H <sub>2</sub>	0.6
C <sub>3</sub> 's and C <sub>4</sub> 's	0.4
H <sub>2</sub> S	43 ppmv
Wet gas (mg/Nm <sup>3</sup> )	
Benzene	6200
"Total tar" (MW>benzene)	13600

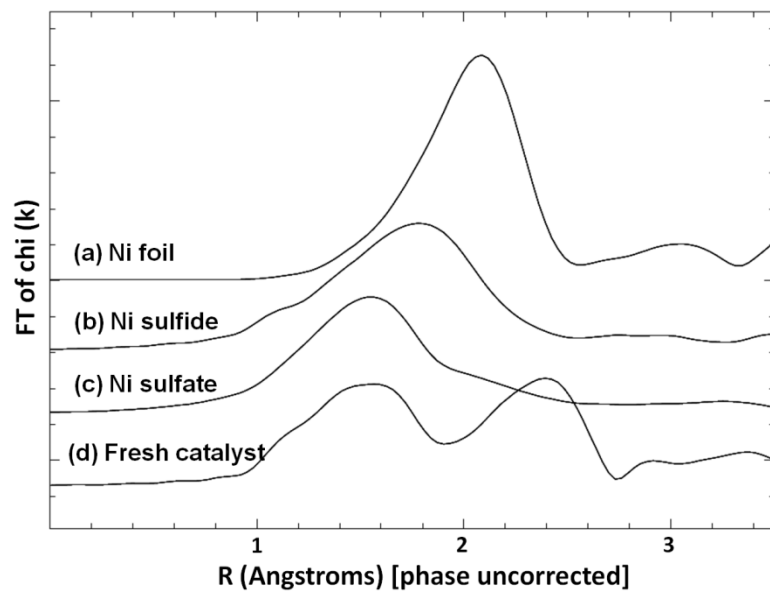


**Figure S1: EXAFS spectra (Fourier transform of EXAFS function) of selected references and a pristinely calcined catalyst (Oxidized (1)) used to develop model for subsequent analysis.**

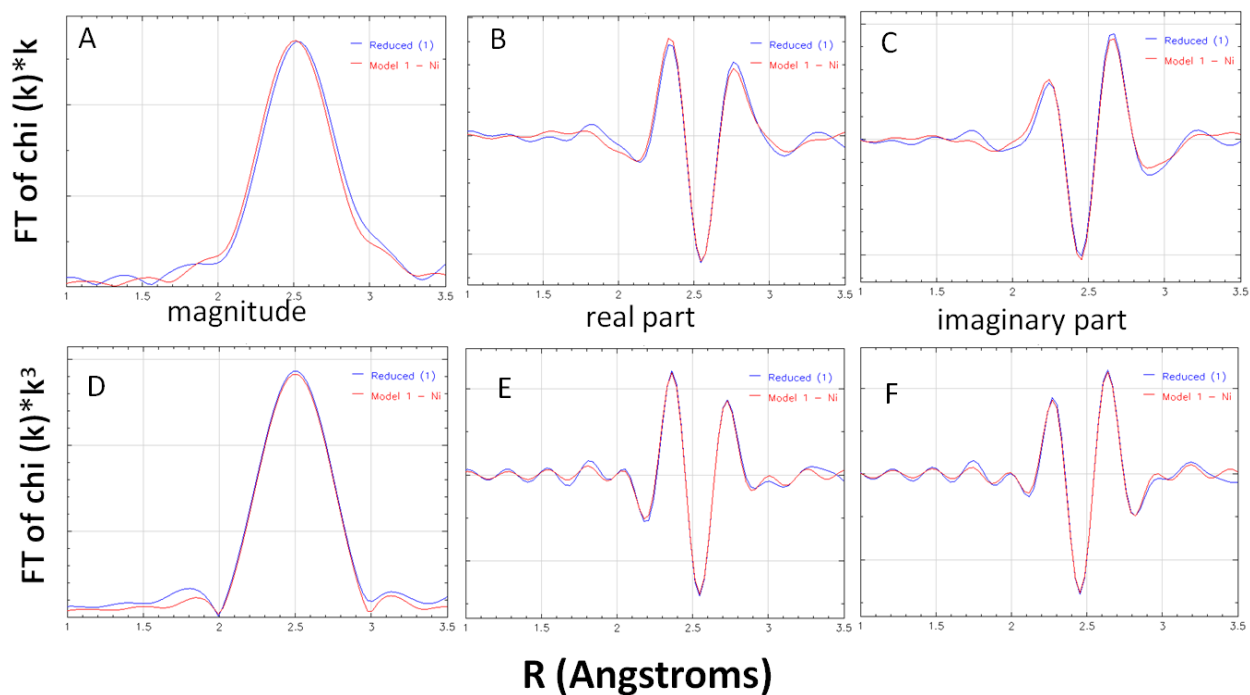


**Figure S2: Results of EXAFS analysis using Ni model (Model 1) for Reduced (1) with  $k^1$ -weighted Fourier transform of EXAFS function in magnitude (A), real part (B), and imaginary part (C) and with  $k^3$ -weighted Fourier transform of EXAFS function in magnitude (D), real part (E), and imaginary part (F).**

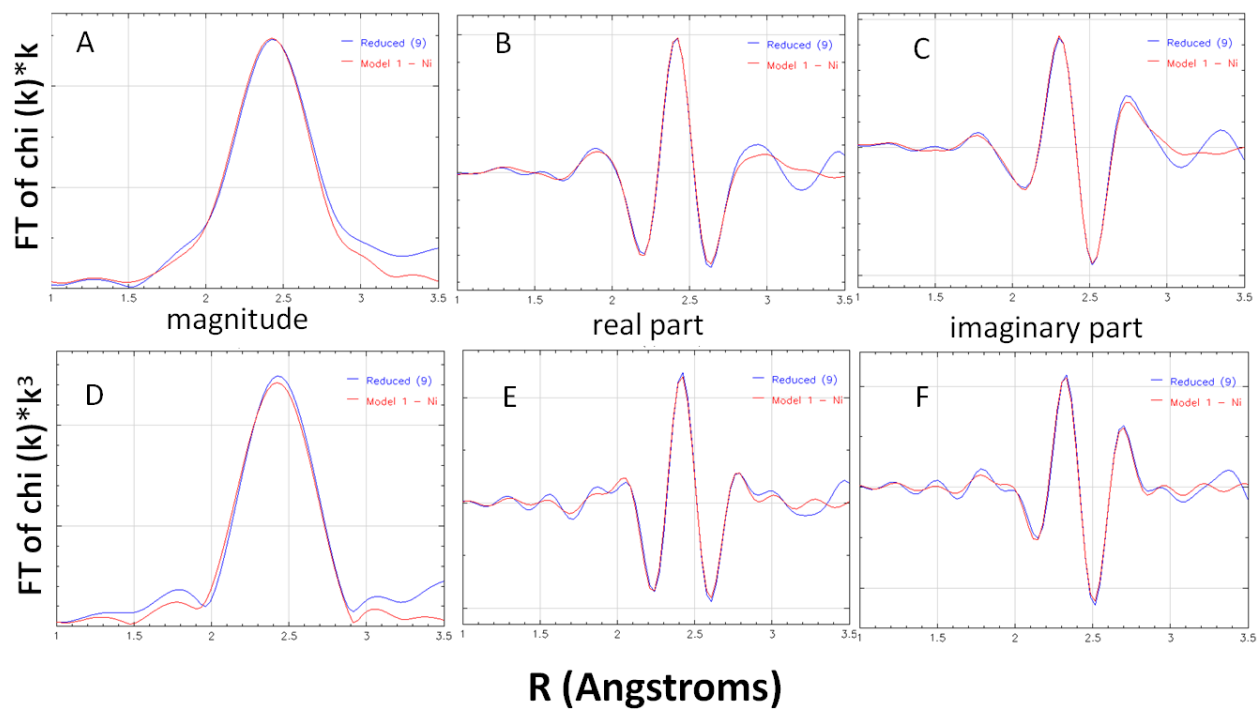


**Figure S3: Results of EXAFS analysis using Ni model (Model 1) for Reduced (9) with  $k^1$ -weighted Fourier transform of EXAFS function in magnitude (A), real part (B), and imaginary part (C) and with  $k^3$ -weighted Fourier transform of EXAFS function in magnitude (D), real part (E), and imaginary part (F).**

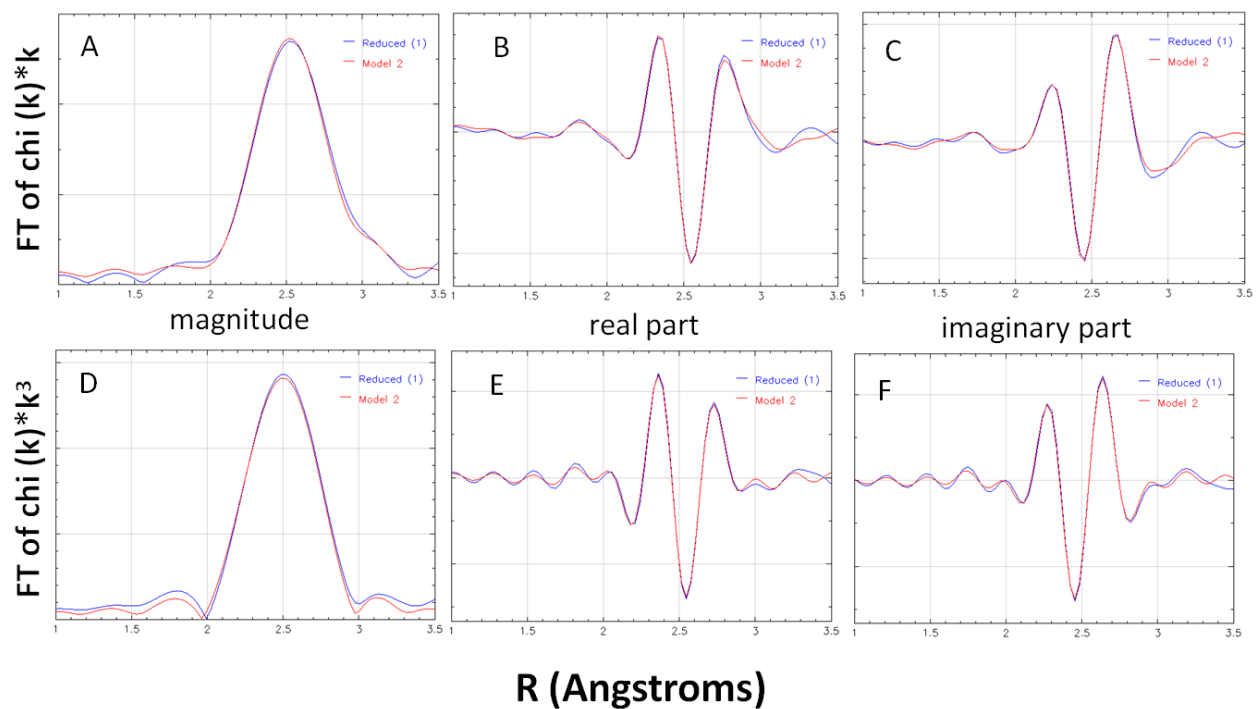


**Figure S4: Results of EXAFS analysis using Ni and oxide model (Model 2) for Reduced (1) with  $k^1$ -weighted Fourier transform of EXAFS function in magnitude (A), real part (B), and imaginary part (C) and with  $k^3$ -weighted Fourier transform of EXAFS function in magnitude (D), real part (E), and imaginary part (F).**

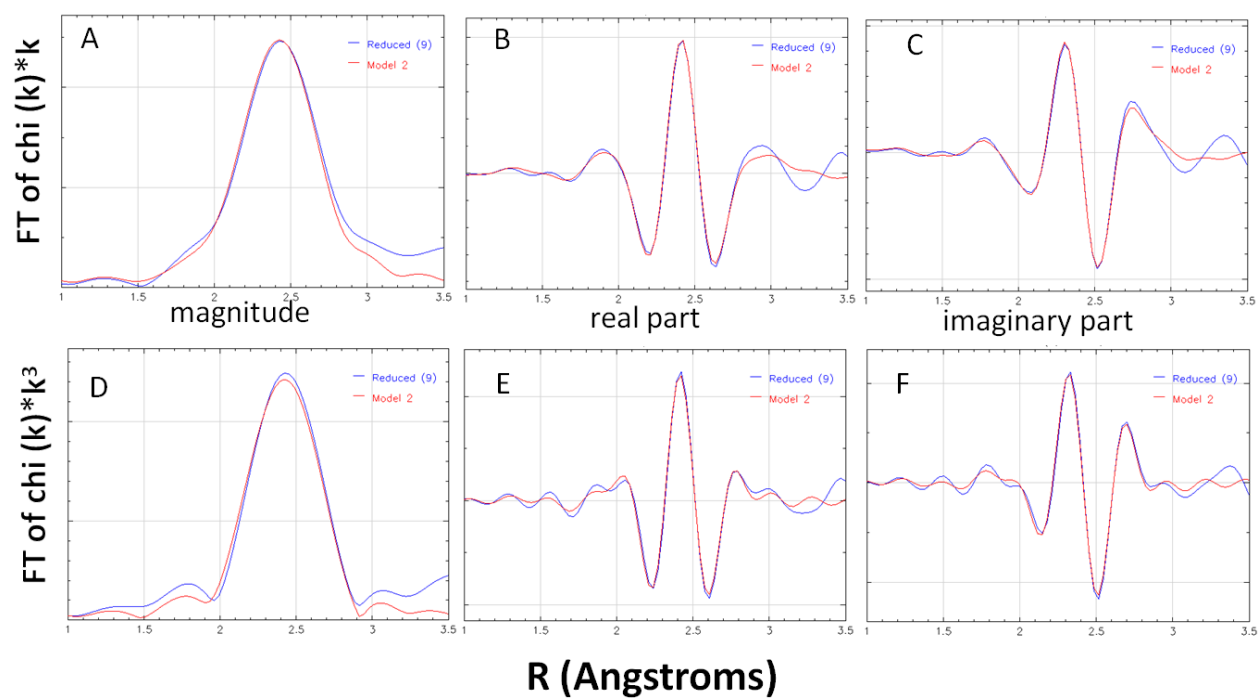


**Figure S5: Results of EXAFS analysis using Ni and oxide model (Model 2) for Reduced (9) with  $k^1$ -weighted Fourier transform of EXAFS function in magnitude (A), real part (B), and imaginary part (C) and with  $k^3$ -weighted Fourier transform of EXAFS function in magnitude (D), real part (E), and imaginary part (F).**

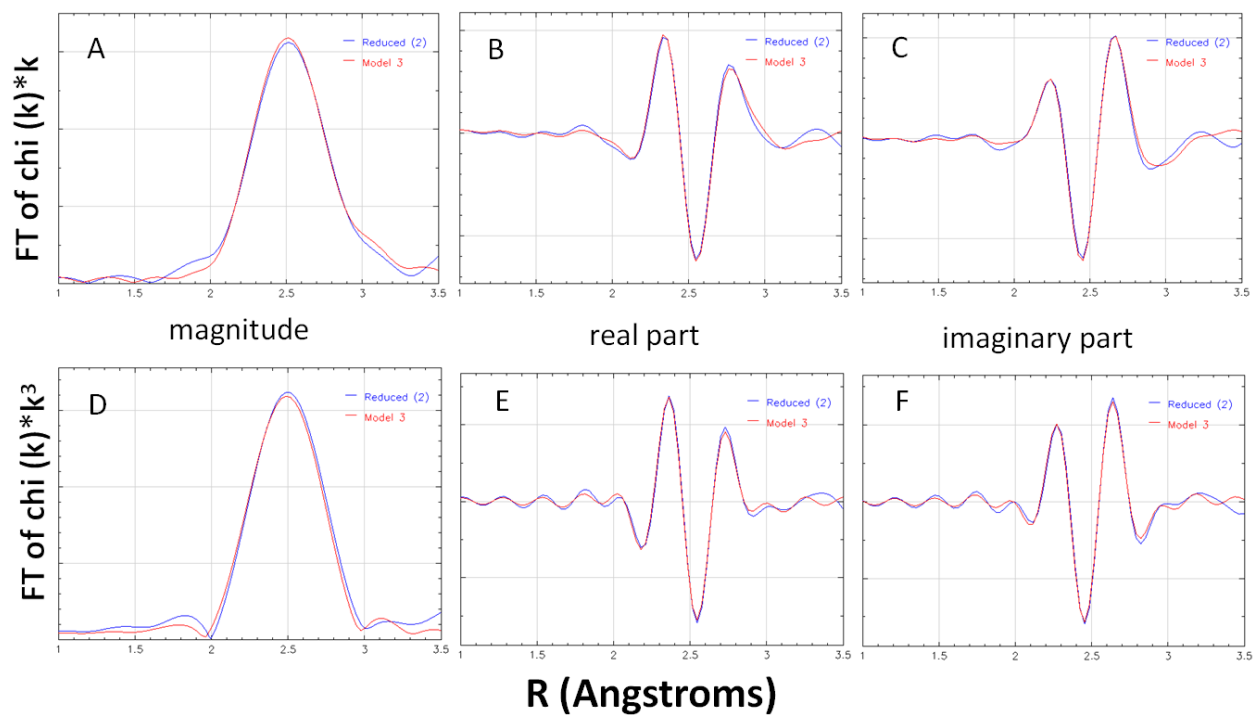


**Figure S6: Results of EXAFS analysis using Ni and sulfide model (Model 3) for Reduced (2) with  $k^1$ -weighted Fourier transform of EXAFS function in magnitude (A), real part (B), and imaginary part (C) and with  $k^3$ -weighted Fourier transform of EXAFS function in magnitude (D), real part (E), and imaginary part (F).**

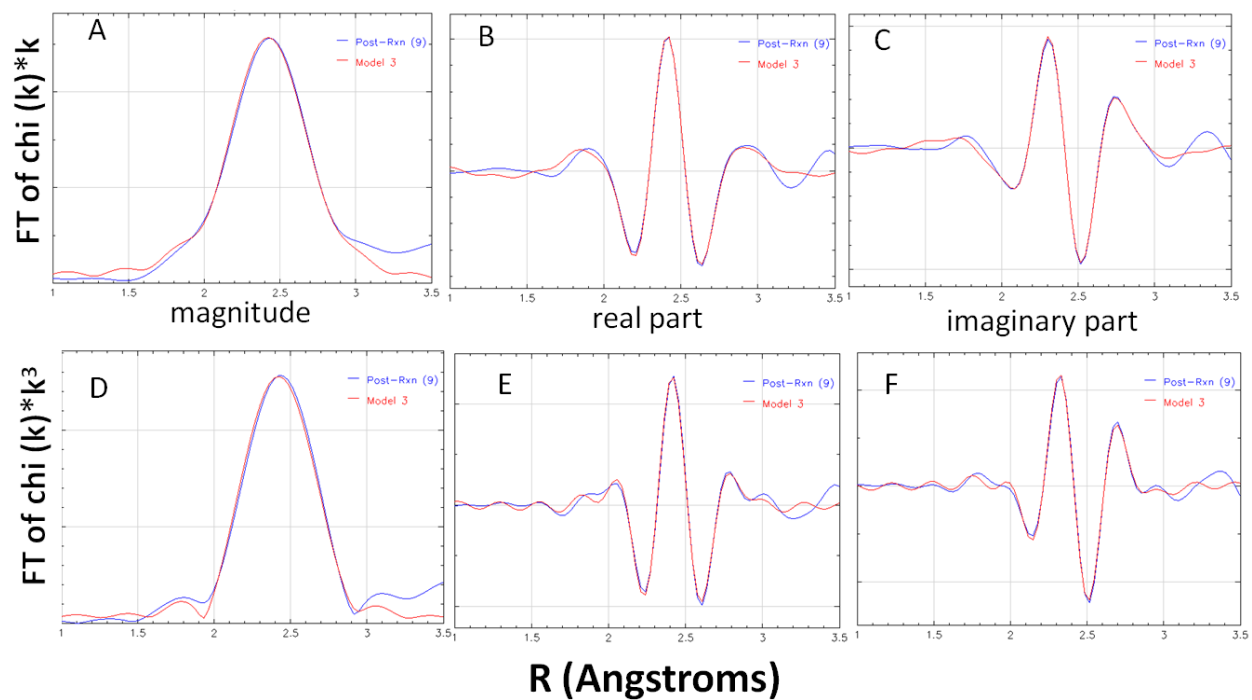


**Figure S7: Results of EXAFS analysis using Ni and sulfide model (Model 3) for Post-Reaction (9) with  $k^1$ -weighted Fourier transform of EXAFS function in magnitude (A), real part (B), and imaginary part (C) and with  $k^3$ -weighted Fourier transform of EXAFS function in magnitude (D), real part (E), and imaginary part (F).**

## Supporting Information References

- (1) Yung, M. M.; Magrini-Bair, K. A.; Parent, Y. O.; Carpenter, D. L.; Feik, C. J.; Gaston, K. R.; Pomeroy, M. D.; Phillips, S. D. *Catalysis Letters* **2010**, *134*, 242–249.
- (2) Ravel, B.; Newville, M. *Journal of Synchrotron Radiation* **2005**, *12*, 537–541.
- (3) Newville, M. *Journal of Synchrotron Radiation* **2001**, *8*, 322-324.
- (4) Rehr, J. J.; Albers, R. C. *Reviews of Modern Physics* **2000**, *72*, 621-654.
- (5) Gibbs, G. V.; Downs, R. T.; Prewitt, C. T.; Rosso, K. M.; Ross, N. L.; Cox, D. F. *Journal of Physical Chemistry B* **2005**, *109*, 21788-21795.
- (6) Yoshida, T.; Tanaka, T.; Yoshida, H.; Funabiki, T.; Yoshida, S. *Journal of Physical Chemistry B* **1996**, *100*, 2302-2309.
- (7) Ferrandon, M.; Kropf, A. J.; Krause, T. *Applied Catalysis A: General* **2010**, *379*, 121-128.
- (8) Clause, O.; Bonneviot, L.; Che, M. *Journal of Catalysis* **1992**, *138*, 195-205.
- (9) Clause, O.; Kermarec, M.; Bonneviot, L.; Villain, F.; Che, M. *Journal of American Chemical Society* **1992**, *114*, 4709-4717.
- (10) Kelly, S. D.; Yang, N.; Mickelson, G. E.; Greenlay, N.; Karapetrova, E.; Sinkler, W.; Bare, S. R. *Journal of Catalysis* **2009**, *263*, 16–33.